# A Vertex Function--Based Radial--Angular Quadrature for the Numerical Evaluation of Surface Test Integrals in the Method of Moments

# A Vertex Function–Based Radial–Angular Quadrature for the Numerical Evaluation of Surface Test Integrals in the Method of Moments

Javier Rivero, Víctor F. Martín, *Member, IEEE*, Donald R. Wilton, *Life Fellow, IEEE*, William A. Johnson, *Senior Member, IEEE*, and Francesca Vipiana, *Senior Member, IEEE*

***Abstract*—A novel integration scheme is proposed for the accurate numerical evaluation of test (reaction) integrals needed for solving complex direct or inverse electromagnetic problems using surface integral equation (SIE) formulations and the method of moments. Significant effort has already been devoted to improving the numerical evaluation of source integrals yielding potentials (or their derivatives), especially for triangular elements. However, numerical techniques for accurately evaluating the subsequent test integrals have been largely neglected, with simple numerical integration schemes being used that either ignore or are developed with incomplete knowledge of the detailed behavior of potentials (or their derivatives) near edges and vertices. Consequently, simple numerical quadrature schemes are found to be either of limited accuracy or slowly convergent with respect to increasing the sampling for self, edge- or vertex-adjacent source, and test triangle pairs. Here, we describe a simple model derived from static potential integrals that properly describes and bounds the potentials and their derivatives near vertices. From it, we are able to construct appropriate, separable radial-angular quadrature schemes that are both exponentially convergent and applicable to all potential forms of interest arising from both EFIE and MFIE operators. Numerical results are presented that demonstrate the wide-ranging applicability and improved convergence rates of the proposed scheme, and these are compared to some previously reported testing schemes. The method's sensitivity to test triangle shape and the ratio choice of angular-to-radial sampling rates is also briefly explored.**

Received 15 May 2024; revised 9 December 2024; accepted 18 February 2025. Date of publication 3 April 2025; date of current version 9 July 2025. The work of Víctor F. Martín was supported in part by Spanish Government and in part by European Recovery Fund Next Generation EU (RD 289/2021 Margarita Salas UEx) under Project MS-26. *(Corresponding author: Francesca Vipiana.)*

Javier Rivero was with the Department of Electronics and Telecommunications, Politecnico di Torino, 10129 Turin, Italy (e-mail: javier.rivero.polito@gmail.com).

Víctor F. Martín was with the Departamento de Tecnologias de Computadores y Comunicaciones, Universidad de Extremadura, 10003 Cáceres, Spain, and also with the Department of Electronics and Telecommunications, Politecnico di Torino, 10129 Turin, Italy. He is now with the Department of Signal Theory and Communications and Telematic Systems and Computing, Universidad Rey Juan Carlos, 28942 Fuenlabrada, Spain (e-mail: victorf.martin@urjc.es).

Donald R. Wilton is with the Department of Electrical and Computer Engineering, University of Houston, Houston, TX 77204 USA (e-mail: wilton@uh.edu).

William A. Johnson resides in Jemez Springs, NM 87025 USA (e-mail: w.johnson24@comcast.net).

Francesca Vipiana is with the Department of Electronics and Telecommunications, Politecnico di Torino, 10129 Turin, Italy (e-mail: francesca.vipiana@polito.it).

Digital Object Identifier 10.1109/TAP.2025.3555888

***Index Terms*—Integral equations, moments method, numerical analysis, singular integrals, vertex functions.**

## I. Introduction

TO ACCURATELY solve direct or inverse electromagnetic problems of complex structures using surface integral equation (SIE) formulations via the method of moments (MoMs), a cost-effective numerical evaluation of double surface reaction integrals is necessary. The accuracy and performance of SIE methods rely heavily on the efficient and accurate evaluation of double surface (reaction) integrals and have been the subject of intense research.

In the evaluation of the source (inner) integral, the earliest studies used singularity subtraction to remove the dominant singular terms from the integrand that could be separately integrated analytically [1], [2], [3]. More recently, singularity cancellation schemes, which used a transform Jacobian to cancel the singularity, were found to be more effective (see [4], [5], [6], [7], [8], [9], [10]). Accelerations using so-called double exponential transformed quadrature rules can, in principle, handle any singularity type [11] but are typically not as efficient as quadrature schemes tailored to the given problem.

Regarding the evaluation of the test (outer) integral, often simple conventional numerical integration schemes are used, assuming that standard numerical integration of the test integral will converge rapidly as the number of integration points increases. Nevertheless, this assertion is not entirely valid. As shown in, e.g., [12] and [13], a brute force evaluation of such test integrals can be very inefficient and surprisingly inaccurate.

Accordingly, Gurel and Ergul [14], [15] developed a singularity extraction method also for the test integral, while, in computing the gradient of Green's function, Yla-Oijala and Taskinen [16] proposed to modify the test integrand to remove the logarithmic singularity of the source integral.

Recently, in [17], [18], [19], [20], [21], [22], and [23], novel methods to evaluate the source and test integrals together have been presented, showing the possibility of achieving machine precision in the 4-D reaction integral evaluation. However, these implementations are nontrivial and may require extensive modifications to an existing MoM code and are usually specific to a Green's function kernel [24], [25].

In this article, we present a novel test integral quadrature scheme designed specifically to handle the singular behavior of so-called vertex functions [26], whose static limit both describes and bounds the source integral behavior. The behavior suggests the use of the 1-D Ma–Rokhlin–Wandzura (MRWlog) [27], [28] samples and weights for handling logarithmic singularities along both radial lines emanating from a common source/test vertex and along angular arcs orthogonal to the radial lines with angles measured from the closest source edges. For some cases (depending on test and source triangle geometries and conductivities), either a radial or angular singularity may not actually be present and the associated integral can be replaced by a Gauss–Legendre (GL) scheme with approximately twice the sampling efficiency.

Vipiana et al. [12] presented a technique applied to the MFIE kernel for test integrals using a Duffy transform and MRWlog scheme. This technique is extended to the EFIE kernel and compared with the novel one developed here. Moreover, we compare the original and the newly proposed scheme with the two approaches presented in [13], where geometrically symmetrical quadrature rules are derived from the logarithmic singularities arising over the test domain for the case of the EFIE. One of our goals is the development of a numerically based (i.e., sample-based) testing approach that is highly convergent, yet independent of the method used for source integration.

This article is structured as follows. Section II reviews some pertinent background information. Section III briefly summarizes the technique presented in [12] and extends it to the EFIE. In Section IV, the general description of the custom integration scheme derived from the vertex function is described. In Section V, several numerical results are presented, and finally, Section VI discusses conclusions and possible extensions of the proposed approach. Preliminary numerical results were recently presented in [29] and [30].

## II. Background

The accuracy and performance of any MoM simulation ultimately rest on the efficient and accurate evaluation of the double surface (reaction) integrals

$$I_{TS} = \int_T \int_S F(\mathbf{r}, \mathbf{r}')\, dS'\, dS \tag{1}$$

where $F(\mathbf{r}, \mathbf{r}')$ is typically expressed as

$$F(\mathbf{r}, \mathbf{r}') = t(\mathbf{r}) g\left(\mathbf{r}, \mathbf{r}'\right)\, b\left(\mathbf{r}'\right) \tag{2}$$

where $t(\mathbf{r})$ is either a scalar or a vector component of a testing function; $b(\mathbf{r}')$ is similarly defined for a basis function; and $g(\mathbf{r}, \mathbf{r}')$ is either a scalar or a scalar component of a vector or dyadic Green's function, with a $\mathcal{O}(|\mathbf{r} - \mathbf{r}'|^{-1})$ or $\mathcal{O}(\nabla|\mathbf{r} - \mathbf{r}'|^{-1})$ singularity. Here, $\mathbf{r}$ denotes the position vector of a test observation point, whereas $\mathbf{r}'$ denotes the corresponding source point quantity. Finally, $S$ is the source integral domain and $T$ is the test domain.

The evaluation of the innermost (source) integral

$$I_S(\mathbf{r}) = \int_S F\left(\mathbf{r}, \mathbf{r}'\right)\, dS' \tag{3}$$

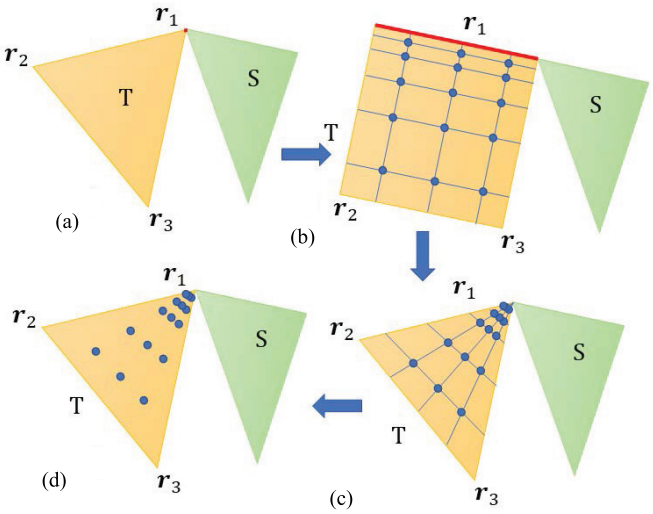


Fig. 1. Quadrature construction steps for a test triangle sharing a common vertex with a source triangle. Original scheme. (a)–(d) Sequence of steps to follow for defining the quadrature points.

can be performed using one of the available methods [4], [5], [6], [7], [8], [9], [10]. In this work, we employ the methods developed in [6] for the EFIE and in [10] for the MFIE, both of which are capable of achieving machine precision for the source integral.[1]

Assuming that the inner integral has been accurately evaluated, we concentrate here on evaluating the outer integral

$$I_{TS} = \int_T I_S(\mathbf{r})\, dS \tag{4}$$

for these critical cases: overlapping, common vertex, and common edge source and test triangles.

## III. Original Testing Scheme

### A. Previous Treatment of the MFIE

Vipiana et al. [12] presented a method for improving the accuracy of the test integrals arising from the MFIE when dealing with triangles sharing a common vertex or edge. It used the Duffy transform, which maps the three edges of a triangle into three edges of a rectangle, with one of its vertices "stretched" into the fourth edge of the rectangle.

In cases where the test and source triangles shared a common vertex, it was assumed that the quadrature rule for the test integration should account for the known logarithmic singularity due to the edge with the shared vertex. To address this singularity, the Duffy transform was applied to the test triangle such that the shared vertex of the test triangle was "stretched" into a newly created edge, forming a rectangular domain. The MRWlog quadrature scheme was then applied along dimensions perpendicular to the new edge with denser sampling near the new edge. Then, for the transverse weights and sample points, the standard Gauss GL quadrature rule was

[1]One should note, however, that evaluating the interaction integrals to machine precision does *not* imply similar convergence of the unknown equivalent current(s) since we also *assume* that $b(\mathbf{r}')$ is piecewise linear, which may not be the case if an edge of $S$ coincides with an edge of the problem model.

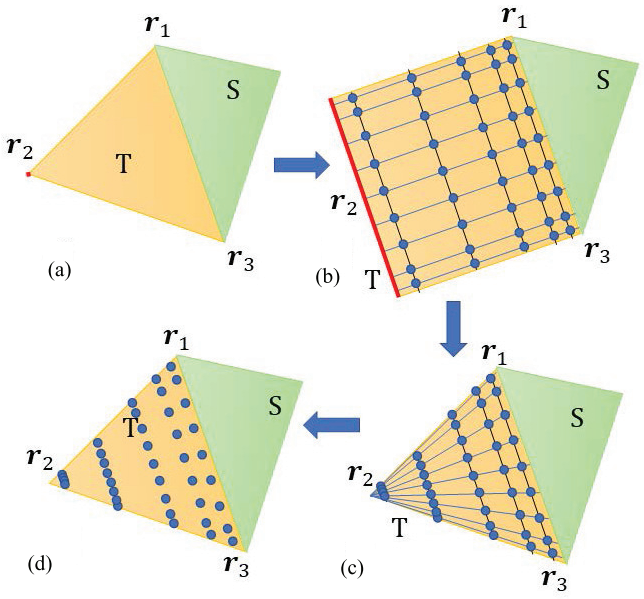


Fig. 2. Quadrature construction steps for a test triangle sharing a common edge with a source triangle. Original scheme. (a)–(d) Sequence of steps to follow for defining the quadrature points.

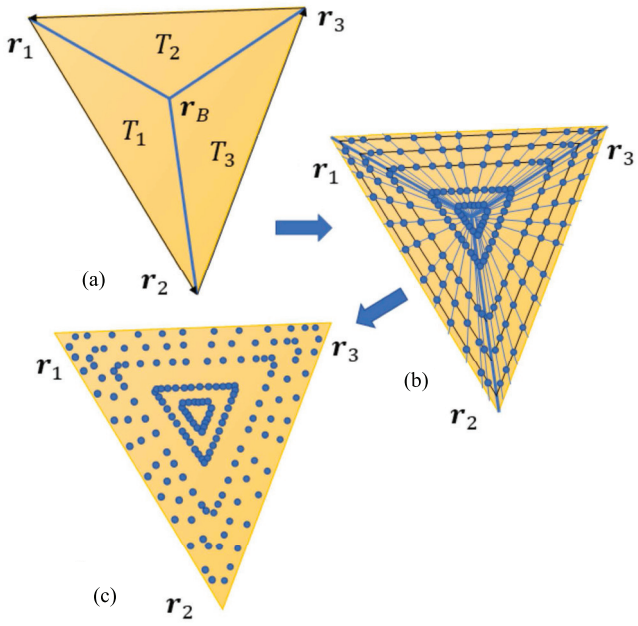


Fig. 3. Quadrature construction steps for a test triangle sharing the domain with a source triangle (self-term). Original scheme. (a)–(c) Sequence of steps to follow for defining the quadrature points.

employed under the assumption that the transverse variations would exhibit a nonsingular behavior. Fig. 1 shows the graphic definition of the test points for a common vertex case.

Instead, for the common edge case, the initial step involved applying the Duffy transform to the test integral with respect to the triangle vertex opposite the edge shared with the source triangle, as shown in the Fig. 2. The Duffy transform maps a test triangle into a rectangular domain. To effectively manage the logarithmic singularity in the integrand near the common edge, we utilized the MRWlog quadrature points. MRWlog defines the weights and sample points in the direction perpendicular to the common edge, corresponding to the radial direction in the original triangular domain. In the direction along the common edge, the quadrature rule must account for a "double" logarithmic singularity, which exists at the two vertices of the common edge. To handle this, the transverse weights and sample points were determined using an extension of the MRWlog quadrature; the new quadrature scheme here mirrors the usual arrangement of MRWlog quadrature points with higher sampling density at one interval endpoint, about a bisector from the free vertex to the middle point of the edge such that the denser sampling occurs nearer the common vertices and far edges. However, a careful inspection of the singular behavior reveals that this is not the best choice. I.e., as we will show here, the source integral also exhibits an *angular* singular behavior at both common vertices, and with the scheme of [12], these singularities were not properly accounted for.

### B. Extension to the EFIE

The original method in [12] was applied to the MFIE only and did not treat the self-term problem. To apply the same scheme to the EFIE, we need only add a scheme for treating self-terms. This can be handled by subdividing the test triangle about its barycenter into three subtriangles, as shown in Fig. 3. Then, each subtriangle is treated as a common edge case, with the barycenter serving as the vertex opposite the common edge for each subtriangle (where the Duffy transformation is applied). An example of the resulting quadrature points obtained with this procedure is reported in Fig. 3(c).

## IV. Proposed Testing Scheme

### A. Brief Development of Vertex Functions

In this section, we develop a custom quadrature scheme to efficiently perform the test integrations (4) over a pair of adjacent planar triangle elements, $S$ and $T$. Our first step is to develop a simple yet robust model that reveals the behavior of the desired potential(s) in the neighborhood of the source triangle $S$, particularly near its edges and vertices. It is found that the so-called static vertex functions [26] provide analytical expressions for the potential functions that capture and bound the essential singularities of potentials near geometrical singularities, i.e., at edges and vertices of subdomains supporting either constant or linear source densities.

Consider a source triangle $S$ with a nearby observation point $\mathbf{r}$. As shown in Fig. 4, $S$ is first split into three *subtriangles*: $q = 1, 2, 3$, about $\mathbf{r}_0$, the projection of $\mathbf{r}$ onto the source plane, by treating $\mathbf{r}_0$ as a new common vertex and connecting new edges to it from the original vertices, and $q = 1, 2, 3$ (index arithmetic in the figure is modulo 3). Note that $\mathbf{r}_0$ needs not fall within $S$. The projection point $\mathbf{r}_0$ is further projected onto each of the three edges (or their extensions), further subdividing the original subtriangles into six right triangles that we refer to as *right subtriangles*.

This successive subdivision scheme depends on the observation point positions $\mathbf{r}$ through its projections and ensures the following. Any (near-)singularities of the potentials (including their derivatives) can only appear at vertices of the right

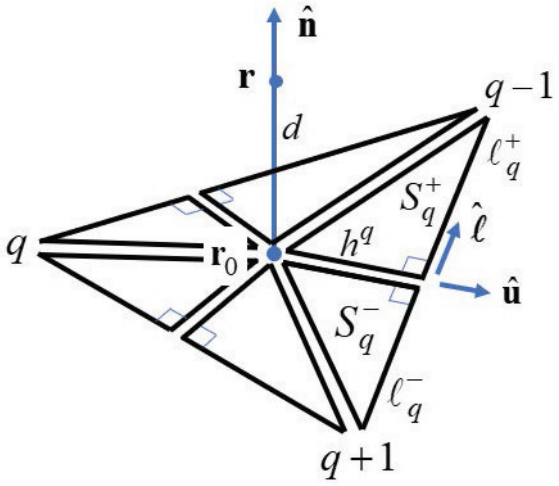


Fig. 4. Source triangle $S$ is split into six right subtriangles about projections of $\mathbf{r}$ first onto the plane and then onto the edges of $S$. The static potentials and their derivatives for constant and linear source densities on each of the resulting right subtriangles can be expressed in closed form and used to suggest efficient testing schemes.

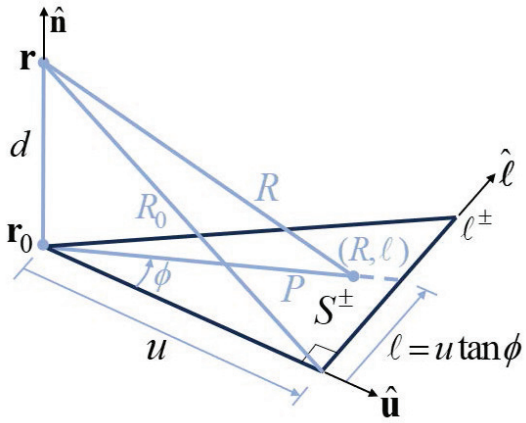


Fig. 5. Coordinates for evaluating vertex function integrals in right subtriangles, $S^{\pm}$.

subtriangles as $\mathbf{r}$ (and hence $\mathbf{r}_0$) moves about. Specifically, for each right subtriangle, a singularity may exist: 1) at the $\mathbf{r}_0$ vertex if $\mathbf{r}$ approaches an interior point of $S$; 2) at the right angle corner if $\mathbf{r}$ approaches an edge of $S$; or 3) at the remaining subtriangle vertex if $\mathbf{r}$ approaches a vertex of $S$. Note that if $\mathbf{r}$ is on an edge of $S$ (i.e., $u = h^q = 0$ and $d = 0$) in Fig. 4, then 2) implies a possible singularity along the edge as well.

As illustrated in Fig. 4, for standard linear bases, the problem thus reduces to the evaluation of potential integrals for constant or linear sources on (up to) six right subtriangles with perpendicular sides of length $u = h^q$ and $\ell = \ell^{q\pm}$, for $q = 1, 2, 3$ and $\mathbf{r}$ an observation point $d$ units above ($d > 0$) or below ($d < 0$) the source plane. In the following, our focus is on the contributions from a pair of right subtriangles associated with a single edge only. Hence, for brevity, in the following, we drop the vertex and edge designating superscripts $q$.

Interestingly, the relevant vertex potential integrands of (3) can all be integrated radially in closed form from $\mathbf{r}_0$ to the opposite edge of each right subtriangle, and the remaining integral is conveniently parameterized in terms of the subtriangle edge lengths $\ell^{\pm}$ of Fig. 4, i.e., from (3) and Figs. 4 and 5, we may write

$$I_{S^{\pm}}(\mathbf{r}) = \int_0^{\tan^{-1}\ell^{\pm}/u} \int_0^{|u/\cos\phi^{\pm}|} F\left(\mathbf{r}, \mathbf{r}'\right) P dP d\phi$$
$$= \int_0^{\ell^{\pm}} \left[ \int_0^{\sqrt{u^2+\ell^2}} \frac{u}{P} F(\mathbf{r}, \mathbf{r}') dP \right] d\ell$$

where $\ell = u\tan\phi$ and the bracketed integral is in closed form. For Rao–Wilton–Glisson (RWG) bases [3] and free-space Green's functions, each vertex function integrand also contains the exponential factor $e^{-jkR} = 1 - jkR - (1/2)k^2R^2 + \cdots$; not surprisingly, only the leading (frequency-independent or *static*) term of this series, together with any other geometrical factors appearing in the integral, determines the singularity orders of the vertex functions. Furthermore, in the static case, even the remaining angular or edge vertex function integrals above can be evaluated in closed form, as in [1], [2], and [26], from which the dominant behavior of the source integrals may be determined as a function of the parameters $u, \ell^{\pm}$, and $d$. All the higher order (frequency-dependent) terms in the exponential expansion will lead to terms with lower order singularities, as can be seen directly in such results as those of [13], [16], and [31]. Furthermore, the singularities are always of logarithmic form and amenable to integration using the so-called MRWlog scheme that exactly numerically integrates functions of the form $P_N(x) + Q_N(x)\ln x$, where $P_N(x)$ and $Q_N(x)$ are polynomials of degree $N$ [27], [28].[2] The approach of Ma, Rokhlin, and Wandzura is a generalized approach that has been applied to other types singularities, such as square roots (MRWsqrt). A significant advantage of the MRW schemes is their simplicity. For integrands of the requisite form (and in contrast to schemes employing auxiliary transforms, for example), only sampled values of the integrand are required.

The above discussion implies that the MRWlog scheme is well equipped to accurately test both the dominant static term as well as the lower order (less singular) frequency-dependent terms arising from the source integration—as long as the electrical sizes ($\max|kR|$) of the integration domains remain sufficiently small that the phase term of the exponential in the integrand does not become oscillatory. Fortunately, these conditions are met for the near-field interactions of essentially all integral equation approaches and kernels.

The geometrical quantities required to define the vertex potential integrals are first defined next and pictured in Figs. 4 and 5. Following that, the dynamic forms of the vertex functions and their static limits for the usual RWG bases associated with EFIE and MFIE operators are summarized in both rectangular $(u, \ell, d)$ and spherical coordinates $(R, \alpha, \beta)$ defined as follows:

$$\ell^{\pm} = \hat{\boldsymbol{\ell}} \cdot (\mathbf{r}^{\pm} - \mathbf{r}_0) = \pm R\cos\alpha$$

[2]Apparently, Crow [32] independently developed the same scheme as the MRWlog scheme, at about the same time. In recent years, the scheme has also been extended to very high orders with the sample points and weights computed to almost 33 significant digits and in agreement with all previously reported results to the precisions and quadrature orders available.

$$u = \hat{\mathbf{u}} \cdot (\mathbf{r}^{\pm} - \mathbf{r}_0) = R_0 \cos\beta = R \sin\alpha \cos\beta$$
$$d = \hat{\mathbf{n}} \cdot (\mathbf{r} - \mathbf{r}^{\pm}) = R_0 \sin\beta = R \sin\alpha \sin\beta$$
$$R_0 = R \sin\alpha = \sqrt{u^2 + d^2}$$

where (see also Figs. 5 and 6)

$$R = \sqrt{u^2 + (\ell^{\pm})^2 + d^2}$$
$$\alpha = \pm \text{atan2}\left(R_0, \ell^{\pm}\right)$$
$$\beta = \text{atan2}(d, u).$$

The four relevant vertex functions are now defined as follows:

$$\begin{aligned} I_{\Phi}(u, \ell^{\pm}, d) &= \int_{S^{\pm}} \frac{e^{-jkR}}{R} dS' \\ &= \int_0^{\ell^{\pm}} \frac{u}{P^2} \left( \frac{e^{-jkR} - e^{-jk|d|}}{-jk} \right) d\ell \\ &\xrightarrow{k\to 0} u \sinh^{-1} \frac{\ell^{\pm}}{R_0} - |d|\, \Omega\left(u, \ell^{\pm}, d\right) \\ &= \pm R \sin\alpha \left( \cos\beta \sinh^{-1}(\cot\alpha) - |\sin\beta| \right. \\ &\qquad \left. \times \tan^{-1}\left( \frac{\cos\alpha \cos\beta}{\sin\alpha + |\sin\beta|} \right) \right) \end{aligned} \tag{5}$$

$$\begin{aligned} I_{\hat{\mathbf{n}}\cdot\nabla\Phi}\left(u, \ell^{\pm}, d\right) &= \partial_d \int_{S^{\pm}} \frac{e^{-jkR}}{R} dS' \\ &= \int_0^{\ell^{\pm}} \frac{ud}{P^2} \left( \frac{e^{-jkR}}{R} - \frac{e^{-jk|d|}}{|d|} \right) d\ell \\ &\xrightarrow{k\to 0} -\text{sgn}(d) \Omega\left(u, \ell^{\pm}, d\right) \\ &= \mp \text{sgn}(\sin\beta) \tan^{-1}\left( \frac{\cos\alpha \cos\beta}{\sin\alpha + |\sin\beta|} \right) \end{aligned} \tag{6}$$

$$\begin{aligned} I_{\hat{\mathbf{u}}\cdot\nabla\Phi}(u, \ell^{\pm}, d) &= \partial_u \int_{S^{\pm}} \frac{e^{-jkR}}{R} dS' \\ &= -\text{sgn}(u) \int_0^{\ell^{\pm}} \frac{e^{-jkR}}{R} d\ell \\ &\xrightarrow{k\to 0} -\text{sgn}(u) \sinh^{-1} \frac{\ell^{\pm}}{R_0} \\ &= \mp \text{sgn}(\cos\beta) \sinh^{-1}(\cot\alpha) \end{aligned} \tag{7}$$

$$\begin{aligned} I_{\hat{\mathbf{u}}\cdot\delta\mathbf{A}}(u, \ell^{\pm}, d) &= \hat{\mathbf{u}} \cdot \int_{S^{\pm}} \frac{e^{-jkR}}{R} (\mathbf{r}' - \mathbf{r}_0) dS' \\ &= \text{sgn}(u) \int_0^{\ell^{\pm}} \left( \frac{e^{-jkR} - e^{-jk|d|}}{-jk} \right) d\ell \\ &\xrightarrow{k\to 0} \frac{\text{sgn}(u)}{2} \left( \ell^{\pm}(R - 2|d|) + R_0^2 \sinh^{-1} \frac{\ell^{\pm}}{R_0} \right) \\ &= \pm \frac{R^2 \text{sgn}(\cos\beta)}{2} \left( \cos\alpha \left(1 - 2\sin\alpha\, |\sin\beta|\right) \right. \\ &\qquad \left. + \sin^2\alpha \sinh^{-1}(\cot\alpha) \right) \end{aligned} \tag{8}$$

where

$$\Omega(u, \ell^{\pm}, d) = \tan^{-1} \frac{u\ell^{\pm}}{R_0^2 + |d|R} = \pm \tan^{-1} \frac{\cos\alpha \cos\beta}{\sin\alpha + |\sin\beta|} \tag{9}$$

is the (signed) solid angle spanned by the right subtriangle with side $\ell^{\pm}$ as viewed from $\mathbf{r}$ [33].

In each case, the first equality merely defines the vertex function for the designated potential quantity as a surface integral over a right subtriangle involving Green's function and either a constant or linear source density. To obtain the next equality, a radial integration is carried out on each right subtriangle; the resultant radial integral then becomes the integrand of the line integral along the source subtriangle edge nearest or in common with the test triangle, $\partial S$. Its quasi-static form is the limit $k \to 0$ of the line integrals, which can be integrated to obtain the closed form shown. The last equality expresses the same result in terms of spherical coordinates with origin at vertex $\ell = \ell^{\pm}$ of the associated right source subtriangle.

In practice, vertex function source integrals are evaluated for *pairs* of right subtriangles associated with the same edge of $S$ (e.g., edge $q$ in Fig. 4) as a difference of anti-derivatives evaluated at endpoints of an edge as $I_{\text{X}}(u, \ell^{+}, d) - I_{\text{X}}(u, \ell^{-}, d)$, with $u = h$ as the common height of the pair, $\ell = \ell^{\pm}$ as the respective right subtriangle edge lengths of the pair for an edge of total length $\ell = \ell^{+} - \ell^{-}$, and for an observation point $d$ units above or below the planar triangle $S$ comprising the six right subtriangles. The subscripts $\text{X} = \Phi, \hat{\mathbf{n}} \cdot \nabla\Phi, \hat{\mathbf{u}} \cdot \nabla\Phi$, and $\hat{\mathbf{u}} \cdot \delta\mathbf{A}$ of the vertex functions $I_{\text{X}}(u, \ell^{\pm}, d)$ of (5)–(8) denote the (static) scalar potential, the normal, and the tangential components of the potential gradient for a constant source density and for a radially varying vector source contribution to the vector potential, respectively. Some of the vertex potentials in (5)–(8) have simpler forms than those found in [26], the main simplification being that terms related to interior edges of a subtriangle cancel with similar terms of adjacent subtriangles of $S$ do not appear in (5)–(8).[3]

### *B. Extracting From Vertex Functions Dominant Potential Singularities Near Isolated Vertices and Edges*

In Section IV-A, we briefly developed and evaluated the static forms of the vertex functions used in computational electromagnetics. Their forms dictate the basic behaviors at vertices and edges that any testing scheme should be able to integrate. In this section, we extract this information from the vertex functions. Once this is done, however, it is important to note that we need no longer be concerned with the method we employ to evaluate the source integrals (though their accuracy should at least be commensurate with that of the testing scheme in order to ensure overall accuracy in MoM matrix elements).

Quantities $(u, \ell,$ and $d)$ and $(R, \alpha,$ and $\beta)$ associated with an observation point at $\mathbf{r}$ in a test triangle $T$ having a vertex

[3]Though the static vertex potential expressions in [26] are all correct, they often do not appear to agree with (5)–(8) when compared term by term. The differences may be attributed to the manner in which they were derived, i.e. using direct integration over *isolated* or *local* subtriangles in [26], but in (5)–(8) first applying a Gauss law in a *global* sense over a parent triangle $S$, then noting that for continuous integrands, subdivision of the parent merely produces artificially induced *interior* edges (see Fig. 4) across which the resulting line integral contributions must cancel, leaving only contributions from *outer* edges, and involving only the (local) normal $\hat{\mathbf{u}}$ components along the outer edges. When summed over all the local subtriangles, in principle, the two approaches must yield identical results. Together, the canceling terms, for example, can often be expressed in the form $\nabla_s \times \mathbf{A}$, which vanishes identically if $\mathbf{A}$ is a gradient, i.e, of the form $\mathbf{A} = \nabla_s \Phi$, as occurs with (6) and (7).

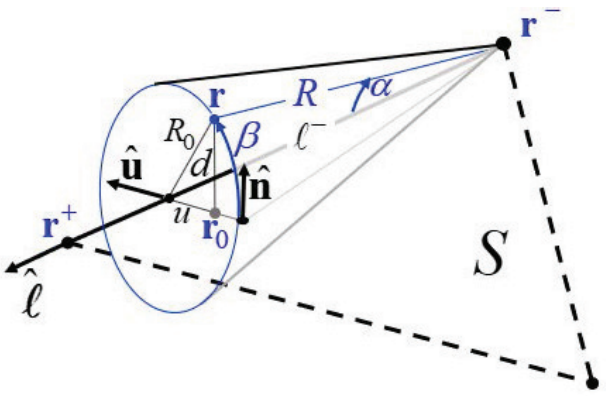


Fig. 6. Highlighted edge (in solid, thick black and gray) of source triangle $S$ is bounded by vertices $\mathbf{r}^-$ and $\mathbf{r}^+$. It is assumed that vertex $\mathbf{r}^-$ is encountered first when traversing the boundary of $S$ in a counterclockwise sense relative to $\hat{\mathbf{n}}$, the unit normal to $S$. The observation point $\mathbf{r}$ is assumed to lie on an arbitrarily oriented test triangle $T$ (not shown) with a common vertex at $\mathbf{r}^-$. $T$ thus contains not only $\mathbf{r}$ but also the radial line from $\mathbf{r}^-$ to $\mathbf{r}$. Angle $\alpha$ is assumed measured from the highlighted edge to the radial line, while the angle $\beta$ is measured about the edge from the half-plane containing $S$ to $\mathbf{r}$. The length $\ell^- = \hat{\boldsymbol{\ell}} \cdot (\mathbf{r}^- \mathbf{r}_0)$ is the signed distance from $\mathbf{r}^-$ to the projection point of $\mathbf{r}_0$ onto the highlighted edge.

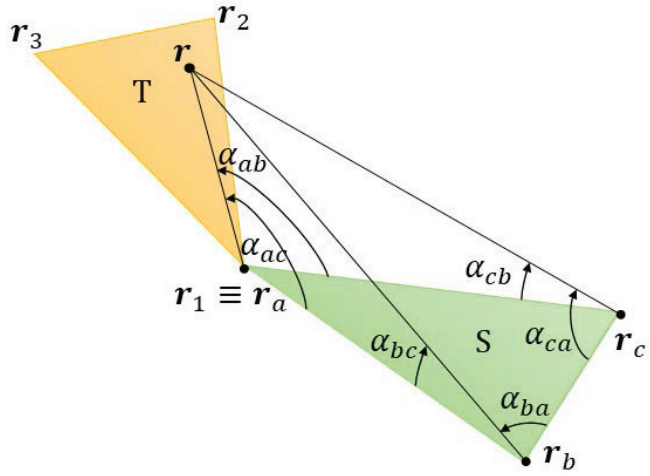


Fig. 7. Vertices of test triangle $T$ are indexed 1–3 and each edge of $T$ is given the same index as that of the corresponding opposite vertex. Similarly for the vertices and edges of source triangle $S$, but with indices $a, b$, and $c$. Position vector $\mathbf{r}$ locates an observation point in $T$, and position vectors $\mathbf{r}_x$, $x \in (1, 2, 3, a, b, c)$ locate the corresponding vertices of $S$ and $T$ where, for the common vertex case shown, $\mathbf{r}_1 = \mathbf{r}_a$. The angle $\alpha_{x,y}$, $x \neq y \in (a, b, c)$, is associated with vertex $x$ of edge $y$ and is measured from edge $y$ to the line connecting $\mathbf{r}$ and $\mathbf{r}_x$.

in common with $\mathbf{r}^-$ of the highlighted edge are illustrated in Fig. 6. Note that $R = |\mathbf{r}^- - \mathbf{r}|$ and $\alpha$ is measured from the edge between $\mathbf{r}^-$ and $\mathbf{r}^+$ (i.e., *not* from either of its extensions beyond $S$). Also, $\beta$ is measured from the half-plane containing $S$. If the observation point $\mathbf{r}$ is in a test triangle $T$ but with its common vertex at $\mathbf{r}^+$ instead, then $R = |\mathbf{r}^+ - \mathbf{r}|$, while the definitions above still apply to measuring $\alpha$ and $\beta$.

In (5)–(8), we note that the solid angle factor $\Omega$ appearing in (5) and (6) satisfies $-2\pi \leq \Omega \leq 2\pi$ and hence is bounded. On the other hand, the vertex functions (5), (7), and (8) involve the term $\sinh^{-1}(\ell^{\pm}/R_0)$ that approaches $\operatorname{sgn}(\sin\alpha)\log(2|\cot\alpha|)$ as $\alpha \to 0$, and hence, vertex potentials containing $\sinh^{-1}$ either become unbounded or have unbounded derivatives, depending on their multiplicative factors. The quantity $\sinh^{-1}(\ell^{\pm}/R_0)$ is constant, however, on any fixed cone such that $\alpha$ is constant, while its multiplicative coefficients may vary with respect to both $\alpha$ and $\beta$. Note that by contrast, the *radial* variation of any static vertex function along a radial line with $\alpha$ and $\beta$ fixed is polynomial-like since each varies as either $R^n, n = 0, 1, 2$.[4]

Fig. 7 shows a test triangle $T$ with vertices 1–3, where vertex 1 is in common with vertex $a$ of source triangle $S$ (with vertices $a, b$, and $c$). Position vectors to the vertices are $\mathbf{r}_x$, $x \in (1, 2, 3, a, b, c)$, where $\mathbf{r}_1 = \mathbf{r}_a$. Each of the six angles $\alpha_{x,y}$, $x \neq y \in (a, b, c)$, is associated with vertex $x$ of edge $y$ and is assumed to be measured from edge $y$ to the line connecting $\mathbf{r}$ and $\mathbf{r}_1$ as shown in the figure. Two vertex functions from each of the three vertices of $S$ contribute to each total potential quantity of interest at the observation point $\mathbf{r}$ in $T$, with most contributions to the total potential at $\mathbf{r}$ varying as either $\log(\cot 2\alpha_{xy})$ (singular) or $\sin(\alpha_{xy})\log(\cot 2\alpha_{xy})$ (singular derivative) for small angles $\alpha_{xy}$, $x \neq y \in (a, b, c)$. A contribution is clearly singular (or has a singular derivative) if any of the associated angles $\alpha_{xy}$ vanish. Referring to the figure, the angles $\alpha_{ay}$, $y = b, c$, are both nonvanishing and constant as $\mathbf{r}$ approaches $\mathbf{r}_1$ along a radial line connecting them, while the angles $\alpha_{xa}$, $x = b, c$, are nonconstant, but also nonvanishing. However, the angles associated with the vertices of $S$ opposite $a$ and that share edges with $a$, i.e., the angles $\alpha_{bc}$ and $\alpha_{cb}$, clearly do vanish as $\mathbf{r} \to \mathbf{r}_1$; hence, their contributions become logarithmically singular near vertex 1 of the test triangle. This suggests using MRWlog quadrature for radial integration on $T$ to properly handle the logarithmically singular contributions (from opposing vertices) there. As $\mathbf{r}$ varies *across* $T$, however, since none of these angles vanish for the common vertex only case, a GL quadrature scheme may be sufficient. Exceptions to this, however, occur in those (perhaps rare) instances when an angle between an edge of $T$ and an edge of $S$ becomes very small (e.g., $\alpha_{x,y} \ll \pi/2$ for some $x, y$). A frequently encountered exceptional case occurs, however, for the common edge case, where $T$ actually shares *two* vertices (and hence a common edge) with $S$. In this case, a singularity in potential (or in its derivative) occurs everywhere along the common edge and at both vertices of the edge. Indeed, for the common edge case, it is best to subdivide the test triangle so as to isolate each of the common edge vertices, treating each test subtriangle separately and using MRWlog quadrature along both radial and (pseudo-)angular directions for each. Note also that since the MRWlog quadrature points are unsymmetrically spaced within its domain, one must orient the sampling both radially and angularly such that higher

[4]It may seem surprising that individual static vertex functions are *constant* or *increasing* with increasing $R$, but this occurs because the source domain (and in the vector potential case, even the source density) also increases with increasing $R$. Hence, the expected $1/R$ or $\nabla 1/R$ static far-field potential behaviors can only result from *cancellations* in summing vertex function contributions over the six source subtriangles. These cancellations render the approach numerically unstable for large $R$. For such cases, it is often preferable to simply integrate by quadrature over both source and test triangles, i.e., over electrically small domains, straightforward numerical integration is inherently a summation process, while evaluating integrals from their anti-derivatives often involves an inherently unstable differencing process.

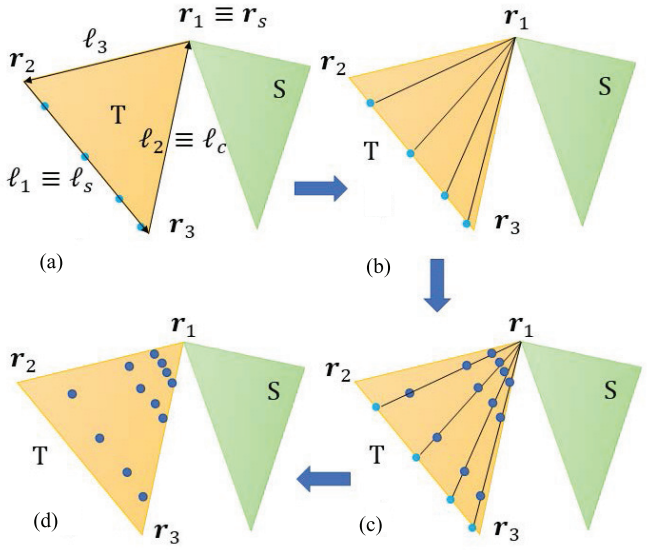


Fig. 8. Quadrature construction steps for a test triangle sharing a common vertex with a source triangle. Proposed scheme. (a)–(d) Sequence of steps to follow for defining the quadrature points.

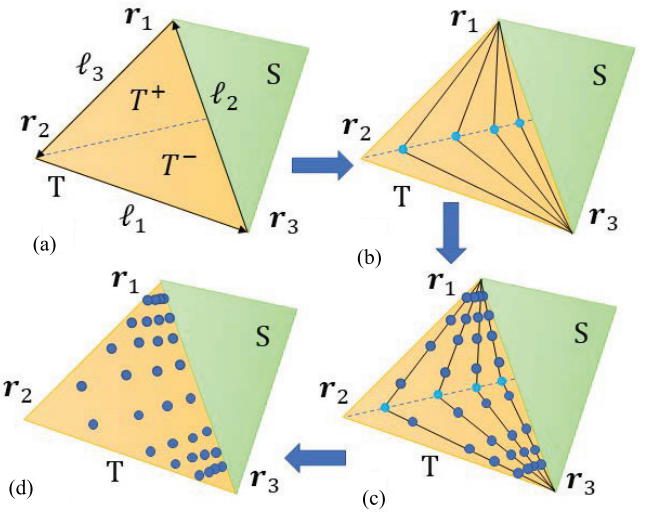


Fig. 9. Quadrature construction steps for a test triangle sharing a common edge with a source triangle. Proposed scheme. (a)–(d) Sequence of steps to follow for defining the quadrature points.

sampling densities occur near (sub)triangle vertices and the common edges. Note that for good convergence, it is not enough to merely sample with higher density near the vertices; we must also properly distribute the points along both the radial and angular directions near each vertex.

### C. Common Vertex Case

We focus first on the common vertex case, as illustrated in Fig. 8. In this case, only one singular region occurs at the test triangle vertex for each source vertex–edge pair attached there. In order to achieve the expected layout of the integration points, we first parameterize the edge opposite the common vertex to form a (pseudo-)angular scheme using MRWlog quadrature points with the higher sampling density nearest the test edge closest to the (nontouching) source edge, as shown in Fig. 8(b). Then, the radial quadrature points use MRWlog with increasing sample density as the common vertex is approached, as illustrated in Fig. 8(c).

An example of the resulting quadrature point distributions obtained via this procedure is shown in Fig. 8(d), where each observation point $\mathbf{r}$ defined on the test triangle can be mathematically expressed as

$$\mathbf{r} = \mathbf{r}_s - \xi_r \left(\boldsymbol{\ell}_c + \boldsymbol{\ell}_s \xi_a\right) \tag{10}$$

where $\xi_r \in (0,1)$ and $\xi_a \in (0,1)$ are the 1-D MRWlog quadrature points used to parameterize the radial and angular directions, respectively; $\mathbf{r}_s$ represents the position vector of the singular (i.e., the common) vertex; $\boldsymbol{\ell}_s$ is the test triangle edge vector defined on the edge opposite the singular vertex; and $\boldsymbol{\ell}_c$ is the test edge vector defined along the closest edge to the source triangle, both defined in the counterclockwise sense on the test triangle as shown in Fig. 8(a). Following the vertex and edge numbering of Fig. 8, these quantities correspond to

$$\mathbf{r}_s = \mathbf{r}_1, \quad \boldsymbol{\ell}_c = \boldsymbol{\ell}_2, \ \boldsymbol{\ell}_s = \boldsymbol{\ell}_1. \tag{11}$$

As the observation point moves from $\mathbf{r}_1$, i.e., the common vertex, toward the opposite edge, $\boldsymbol{\ell}_1$, the point density of the MRWlog radial points, $\xi_r$, decreases, as shown in Fig. 8(c). As the observation point moves from the edge closer to the source triangle, $\boldsymbol{\ell}_2$, toward $\boldsymbol{\ell}_3$, the angular density of points $\xi_a$ in the MRWlog scheme decreases, as shown in Fig. 8(b).

Then, the integral (4) can be calculated as

$$I_{TS} \cong \mathcal{J} \sum_a \sum_r w_a \, w_r \, I_S \left(\mathbf{r}^{(a,r)}\right) \tag{12}$$

where $a$ and $r$ index the selected angular and radial quadrature points, respectively; $w_a$ and $w_r$ are the quadrature weights; and $\mathcal{J} = 2A$ (with $A$ the area of the test triangle) is the Jacobian of the transformation between global and parametric coordinates on the test triangle.

### D. Common Edge Case

For source and test triangles with common edges, two singular regions appear within the edge-adjacent test triangle, one caused by each source vertex–edge pair. The definition of the quadrature points for this case can be followed in Fig. 9. To treat both singular regions, we first split the test triangle into two subtriangles [$T^+$ and $T^-$ as shown in Fig. 9(a)] about the line from the middle (centroid) of the common edge to the opposite vertex. Then, we apply the scheme previously described for the common vertex case (10) independently on each of the two newly created subtriangles. The line from the middle of the common edge to the opposite vertex now becomes the edge opposite the common vertex for both subtriangles. This line is parameterized using MRWlog points, as shown in Fig. 9(b). Finally, considering these points as endpoints, we add sample points radially from each common vertex, using the MRWlog point distribution to form a double radial–angular scheme, as shown in Fig. 9(c).

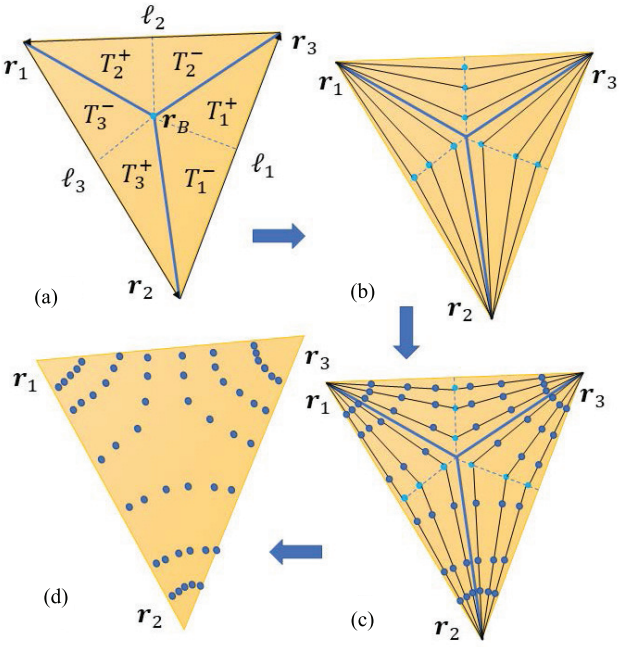


Fig. 10. Quadrature construction steps for a test triangle sharing the domain with a source triangle (self-term). Proposed scheme. (a)–(d) Sequence of steps to follow for defining the quadrature points.

To mathematically define an observation point using the described quadrature [see an example of quadrature points in Fig. 9(d)], we apply (10) to each $T^+$ and $T^-$ triangle [see Fig. 9(a)]; thus, the parameters $\mathbf{r}_s$, $\boldsymbol{\ell}_c$, and $\boldsymbol{\ell}_s$ can be assigned as

$$T^+\colon \mathbf{r}_s = \mathbf{r}_1, \quad \boldsymbol{\ell}_c = \frac{1}{2}\boldsymbol{\ell}_2, \ \boldsymbol{\ell}_s = \frac{1}{2}(\mathbf{r}_1 + \mathbf{r}_3) - \mathbf{r}_2$$
$$T^-\colon \mathbf{r}_s = \mathbf{r}_3 \quad \boldsymbol{\ell}_c = -\frac{1}{2}\boldsymbol{\ell}_2, \ \boldsymbol{\ell}_s = \frac{1}{2}(\mathbf{r}_1 + \mathbf{r}_3) - \mathbf{r}_2 \tag{13}$$

where $\boldsymbol{\ell}_s$ is the vector from $\mathbf{r}_2$ to the midpoint of the common edge of both triangles and $\boldsymbol{\ell}_c$ is the vector defined over the common edge. Note the change of sign of $\boldsymbol{\ell}_c$ relative to that in $T^+$ when applying expression (10) to $T^-$ because $\boldsymbol{\ell}_c$ is chosen to point *toward* the singular vertex $\mathbf{r}_s = \mathbf{r}_3$.

### E. Self-Term Case

The self-term case has six singular regions, one for each vertex–edge pair. The definition for the corresponding quadrature points follows as in Fig. 10. For this case, we first split the triangle into three subtriangles ($T_1$–$T_3$) with common vertex at the barycenter $\mathbf{r}_B = (\mathbf{r}_1 + \mathbf{r}_2 + \mathbf{r}_3)/3$, as shown in Fig. 10(a). We denote each subtriangle $T_i$, $i = 1, 2, 3$, with associated edge vectors, $\boldsymbol{\ell}_i$. Each subtriangle is then parameterized just as for the common edge case (shown in Fig. 9). In other words, each subtriangle is split in two from the middle of the common edge to the barycenter, providing six right subtriangles, as shown in Fig. 10(a). In turn, the resulting right subtriangle is parameterized using the procedure of the common vertex case (shown in Fig. 8).

Finally, an observation point defined on each subtriangle can be mathematically expressed following the same procedure as in the previous cases by applying (10) to each right subtriangle. We can generalize the parameters at each subtriangle $T_i$, with $i = 1, 2, 3$, as

$$T_i^+\colon \mathbf{r}_s = \mathbf{r}_{i+2}, \quad \boldsymbol{\ell}_c = \frac{1}{2}\boldsymbol{\ell}_i, \ \boldsymbol{\ell}_s = \frac{1}{2}(\mathbf{r}_{i+2} + \mathbf{r}_{i+1}) - \mathbf{r}_B$$
$$T_i^-\colon \mathbf{r}_s = \mathbf{r}_{i+1}, \quad \boldsymbol{\ell}_c = -\frac{1}{2}\boldsymbol{\ell}_i, \ \boldsymbol{\ell}_s = \frac{1}{2}(\mathbf{r}_{i+2} + \mathbf{r}_{i+1}) - \mathbf{r}_B \tag{14}$$

where $(\mathbf{r}_{i+2} + \mathbf{r}_{i+1})/2$ is the midpoint of each subtriangle edge. In (14), the index arithmetic is performed modulo three. Note the change in the sign of $\boldsymbol{\ell}_c$ in the right subtriangle $T_i^-$ relative to subtriangle $T_i^+$, as in the common edge case (13).

## V. Numerical Results

In order to examine the accuracy of the proposed test integration scheme, we analyze the convergence behavior of the integral (4) for different sets of triangles, considering three different configurations: a test triangle sharing a common vertex with the source triangle, a test triangle sharing a common edge with the source triangle, and a self-term case where the test and the source domains are coincident. We first ensure for each simulation that the *source* integral in (3) is accurately evaluated to machine double precision by performing all the evaluations using very high order quadratures (tabulated in quad precision), but then in the calculations limiting the results to 16 digits. We also use the radial angular singularity cancellation scheme [6] for the evaluation of the EFIE integrals, and the hybrid subtraction-cancellation procedure described in [10] for the evaluation of the integrals arising in the MFIE. The reference values for the test integrals are computed applying the proposed scheme and our highest order available MRWlog quadrature rule (128 sample points) achieving a reference value accuracy of no less than 16 significant digits.

In all the following numerical results, we compare the proposed and original schemes, labeled as such, to the standard Gauss triangle scheme, labeled as "GT" [34] and the two symmetric logarithmic triangle quadrature rules presented in [13], labeled "ST1" for the approach 1 and "ST2" for approach 2. These two methods have been designed for modeling the singular behavior of the EFIE integrals; in this article, we also apply them for solving the MFIE integrals, and in all the numerical reported results, the number of quadrature sample points used are up to the highest value available in [13]. Moreover, the integration domain is a test triangle with a maximum edge of about $\lambda/5$ (where $\lambda$ is the working wavelength), and the chosen basis functions are RWG basis functions. The aspect ratio (AR) of all the considered test triangles, defined here as the ratio between the triangle height and the length of the closest edge to the source triangle, is 0.5.

The integral evaluation accuracy is measured in terms of the number of significant digits of the computed integral

$$\mathrm{SD}(K) = -\log\left(\left|\frac{I_{\mathrm{ref}} - I_K}{I_{\mathrm{ref}}}\right| + \delta\right) \tag{15}$$

where $I_K$ and $I_{\mathrm{ref}}$ are the evaluated integrals with $K$ sample points and with the highest number of sample points (reference), respectively. The term $\delta = 10^{-16}$ is inserted in (15) in order to merely limit the claimed precision to no more than 16 digits (double precision).

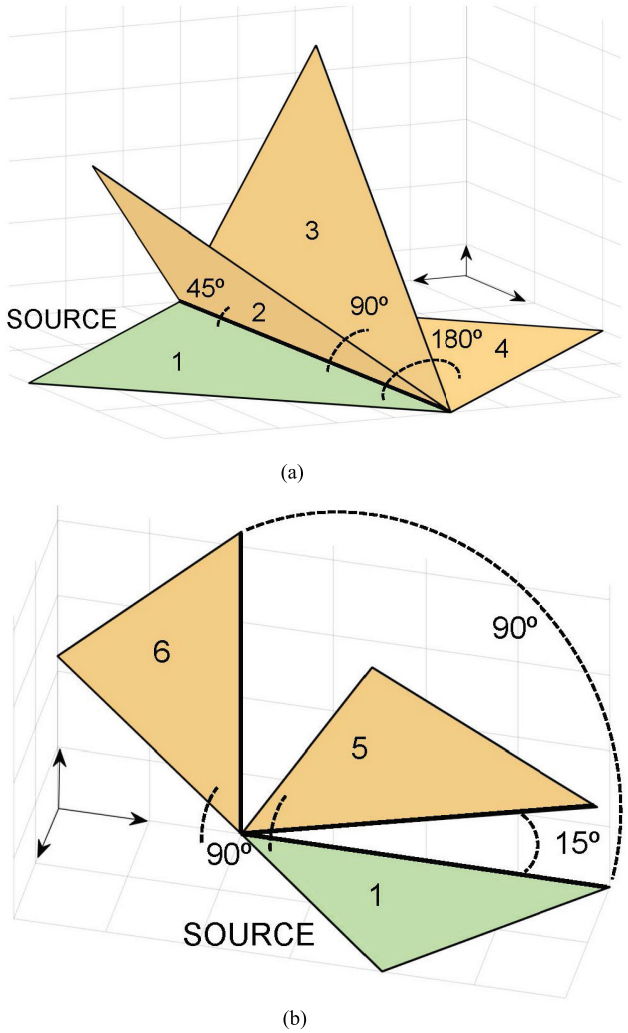


Fig. 11. Triangle configurations for the common edge and common vertex cases. For each case, both the source and test triangles are isosceles triangles with a 2-m base and a height-to-base AR of 0.5. In common edge case (a), their base edges are shared; in common vertex case (b), the source and test triangles share a base vertex from each. The working wavelength used for all convergence comparison studies is $\lambda = 10$ m.

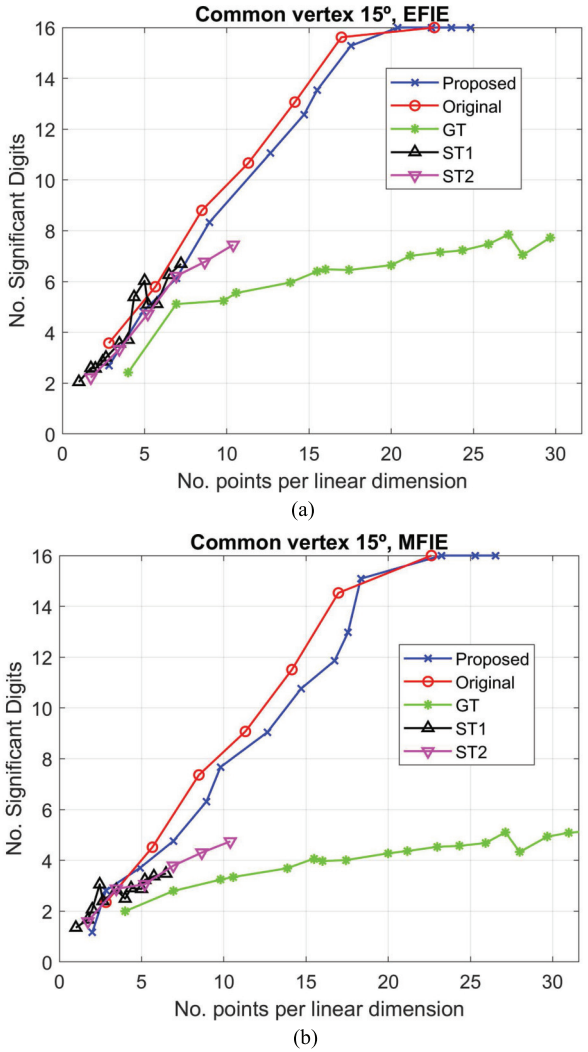


Fig. 12. Number of significant digits versus number of quadrature points per linear dimension; coupling between triangles "1" and "5" in Fig. 11(b). Comparison between the GT quadrature rule, the original method, the ST1 method, the ST2 method, and the proposed method for the integrals belonging to (a) EFIE and (b) MFIE.

In all the following graphs, the obtained SD is reported with respect to the number of quadrature sample points per linear dimension, i.e., equal to $\sqrt{K}$ since we are performing a 2-D surface integral. The relation between the number of radial and angular points is selected to obtain optimal convergence in all cases; in the case of a different number of quadrature sample points between the two directions, i.e., $K_1$ and $K_2$, $\sqrt{K} = \sqrt{K_1 K_2}$. At the end of this section, a preliminary study is included that provides a rough guide to choosing a near-optimal selection of the ratio of $K_1$ and $K_2$ for good accuracy.

### A. Accuracy Analysis for Different Triangle Configurations

We first study the interaction integrals between a source and test pair in the common vertex configuration of Fig. 11. The source and test triangles, labeled "1" and "5" or "6," respectively, are described in the figure; the basis function on each is the RWG basis associated with the closest edges of the pair (hence it is nonvanishing at the common vertex). The closest edges are highlighted in Fig. 11(b). In the two configurations considered, the test triangle lies in the plane containing the test edge and is orthogonal to the source plane. Figs. 12 and 13 show the accuracy in evaluating the interaction integrals between source triangle "1" and test triangles "5" and "6," respectively, for interactions employing both (a) EFIE and (b) MFIE operators in each case. Note that the minimum edge angle separation for the two cases is 15° and 90°, respectively.

It is evident that the proposed and original schemes outperform the usual GT scheme. We observe that, in the case of the EFIE, the GT provides reasonable convergence for low-moderate accuracies, but for higher accuracies, the convergence rate worsens, and only the original and proposed methods are able to achieve machine precision, requiring about 15–20 points per linear dimension. We can see that even the symmetrically distributed points of the ST1 and ST2 methods capture the logarithmic behavior of the EFIE integrals with a convergence similar to the proposed and

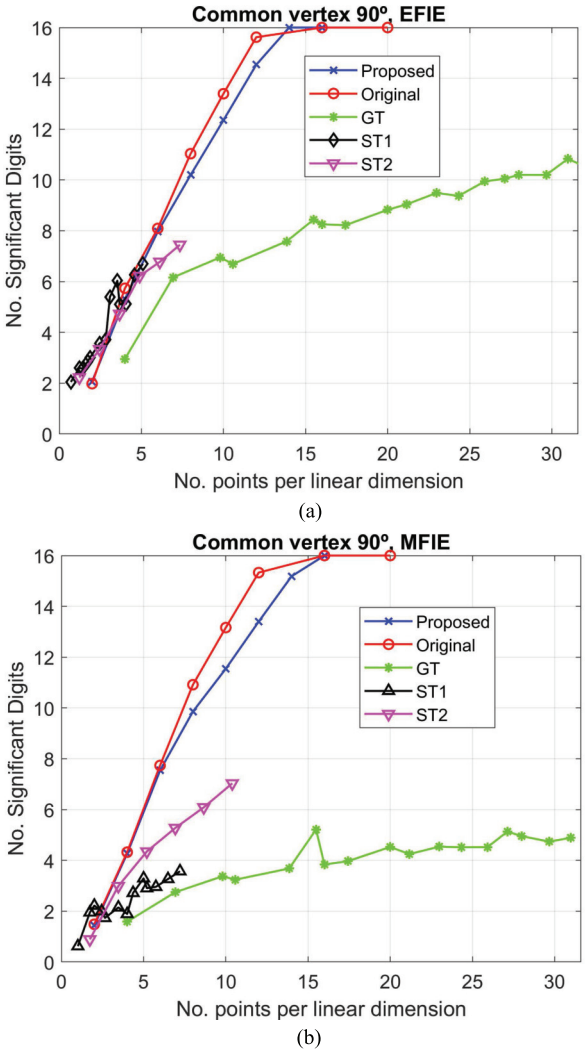


Fig. 13. Number of significant digits versus number of quadrature points per linear dimension; coupling between triangles "1" and "6" in Fig. 11(b). Comparison between the GT quadrature rule, the original method, the ST1 method, the ST2 method, and the proposed method for the integrals belonging to (a) EFIE and (b) MFIE.

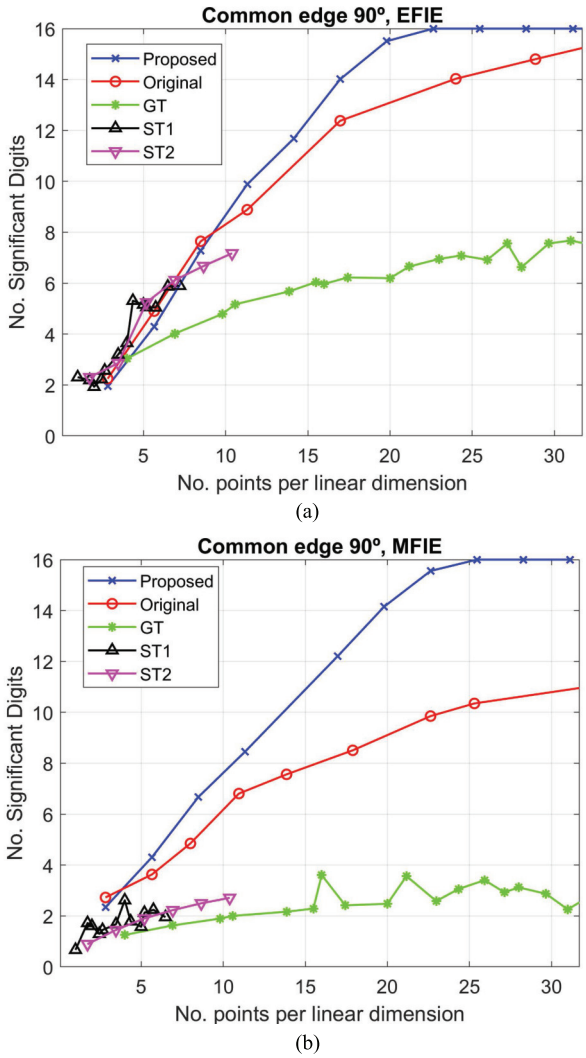


Fig. 14. Number of significant digits versus number of quadrature points per linear dimension; coupling between triangles "1" and "3" in Fig. 11(a). Comparison between the GT quadrature rule, the original method, the ST1 method, the ST2 method, and the proposed method for the integrals belonging to (a) EFIE and (b) MFIE.

original methods. Regarding the integrals belonging to the MFIE, the behavior of the proposed and original schemes are similar, and the dramatic improvement with respect to GT is even more evident, which, in this case, exhibits a loss of up to eight significant digits with respect to the proposed scheme. Moreover, the convergence of the ST1 and ST2 methods is poorer than for the proposed and the original methods, as both the ST1 and ST2 methods were designed around the EFIE.

Next, we characterize the performance of the methods for evaluating the test integrals on a triangle sharing a common edge with the source triangle. Three different cases are considered where the source triangle, labeled "1," is coupled with the test triangles "2," "3," and "4" [shown in Fig. 11(a)]. The selected RWG functions are associated with the common edge. Fig. 14 shows the accuracy in evaluating the integrals belonging to the EFIE (a) and MFIE (b) in the case of triangles "1" and "3," which form an angle of 90°. It can be observed that both the proposed and original approaches exhibit a dramatic performance improvement compared with the GT for both EFIE and MFIE integrals. However, although the convergence of both the proposed and original approaches is similar for low-to-moderate accuracy, the proposed method exhibits exponential convergence, reaching machine precision in around 20 points per linear dimension. Concerning the ST1 and ST2 methods, the results are consistent with the previous examples, exhibiting good convergence for the EFIE integrals, similar to the proposed and original schemes, but with a significant loss of accuracy when evaluating the MFIE integrals. It is important to point out that the convergence of the original scheme is comparable to the convergence of the proposed scheme when applied to the electric equation, but a loss of accuracy of up to four digits can be observed for the first when applied to the magnetic equation. Note also that convergence of the GT scheme stagnates at about seven significant digits for the EFIE and about 3 for the MFIE as the number of quadrature sample points increases.

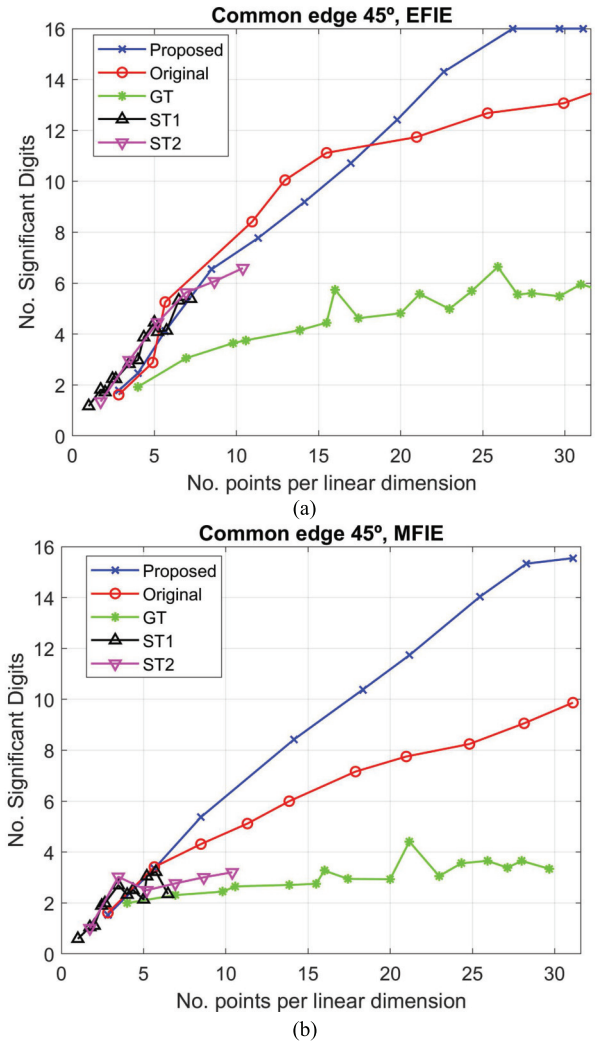


Fig. 15. Number of significant digits versus number of quadrature points per linear dimension; coupling between triangles "1" and "2" in Fig. 11(a). Comparison between the GT quadrature rule, the original method, the ST1 method, the ST2 method, and the proposed method for the integrals belonging to (a) EFIE and (b) MFIE.

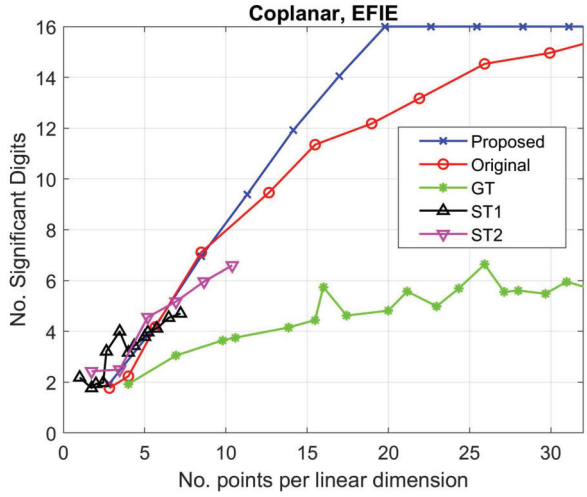


Fig. 16. Number of significant digits versus number of quadrature points per linear dimension; coupling between triangles "1" and "4" in Fig. 11(a). Comparison between the GT quadrature rule, the original method, the ST1 method, the ST2 method, and the proposed method for the integrals belonging only to the EFIE.

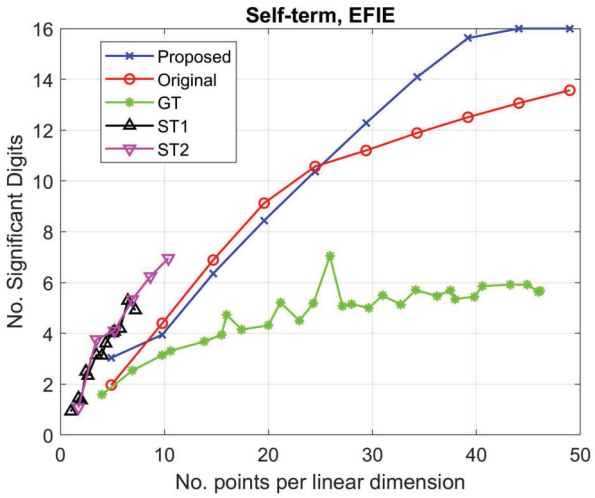


Fig. 17. Number of significant digits versus number of quadrature points per linear dimension; self-coupling of triangle "1' in Fig. 11(a). Comparison between the GT quadrature rule, the original method, the ST1 method, the ST2 method, and the proposed method for the integrals belonging to the EFIE.

A similar picture is observed in Fig. 15 for the case of triangles "1" and "2" [shown in Fig. 11(a)], which form an angle of 45°. All schemes generally exhibit a slower convergence rate, but the proposed method still achieves exponential convergence to machine precision. Moreover, what stands out is the excellent stability of the proposed method, both for the evaluation of the EFIE and MFIE integrals.

The last configuration for the common edge case study involves the coplanar triangles "1" and "4" [shown in Fig. 11(a)]. This case is notable for the original scheme, because although its capability was demonstrated in [12] for the MFIE integrals, it has not been applied to calculating the coupling between two coplanar triangles (whose interactions vanish for the MFIE). The behaviors of the various methods for this example are shown in Fig. 16. We observe a behavior similar to the orthogonal case (see Fig. 14), where all the non-polynomial methods (including those proposed) dramatically outperform the GT scheme, with the proposed scheme being the fastest to achieve machine precision, at around 20 points per linear dimension, and with an exponential convergence rate.

Finally, we study the behavior of the proposed method for the coupling between two RWG basis functions defined within the same triangle, that is, the triangle labeled with "1" in Fig. 11, and the considered RWG basis function is that associated with the highlighted edge in the same figure. This is a very representative example to show the capabilities of the methods because they are able to be applied to improve the performance of the singular integrals arising in the self-terms of the EFIE, which are not present in the MFIE. The convergence for this case is shown in Fig. 17, where it is observed that, as expected, the average number of needed points increases due to the multiple singularities present.

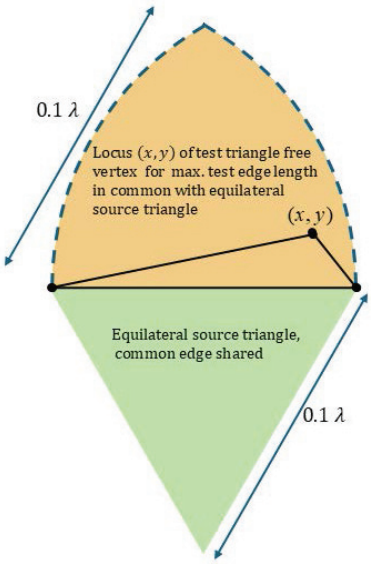


Fig. 18. Example of shape variation of the test triangle. The source triangle (green) is fixed equilateral with $0.1\lambda$ edge length. The test triangle shares a common edge with the source triangle. The noncommon edges vary from $0.002\lambda$ to $0.1\lambda$ edge length, locating the free vertex in the beige area, and generating test triangles whose edges are no longer than their common edge of length $0.1\lambda$.

However, the proposed schemes provide a faster convergence than the GT scheme and are able to achieve machine precision. We also see that although the convergence rate of the proposed scheme is exponential, in this case methods such as ST1 and ST2, which are not exponentially convergent can be more efficient choices for low-to-moderate required accuracies.

### B. Stability Study With Respect to Test Triangle Shape

In previous examples, all test triangles were isosceles with a fixed AR of 0.5. In order to characterize the overall performance of the methods when applied to a realistic problem in a MoM solver, the stability of evaluations with respect to different-shaped test triangles is next investigated. For the sake of conciseness, this study is carried out only for triangles sharing a common edge. For this, we perform a comparison between the number of significant digits obtained in each case for a set of test triangles with different shapes, as shown in Fig. 18. For this case, the source triangle is fixed with equal edge lengths of $0.1\lambda$ and the test triangle shape is changed by varying the noncommon edges from 0.002 to $0.1\lambda$. This analysis is performed using the proposed and original methods for the evaluation of the integrals arising in the EFIE; very similar results have been obtained for the MFIE but are not included here for the sake of conciseness.

The results are shown in Fig. 19. The plot shows the accuracy behavior for 128 quadrature sample points (eight points in angular dimension and 16 points in radial dimension) for the original and the proposed schemes versus the test triangle shape, as shown in Fig. 19(a) and (b), respectively. The color at each point $(x, y)$ represents the number of significant digits for the test triangle with the free vertex located at that point. In general, the obtained results are quite stable, showing a limited

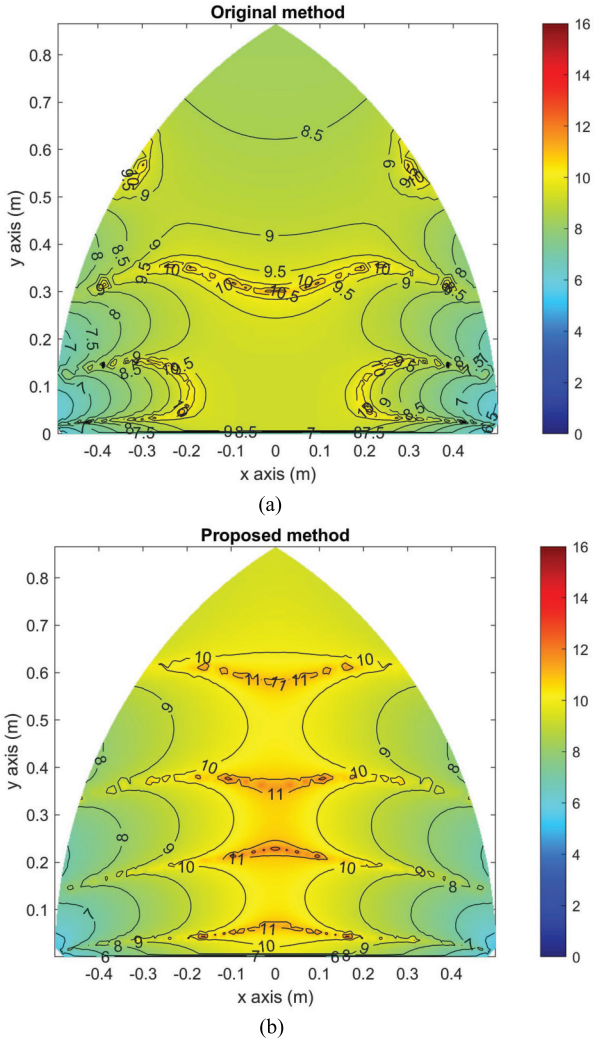


Fig. 19. Number of significant digits versus different test triangle shapes; the color at each point $(x, y)$ represents the number of significant digits for the test triangle with the free vertex located at that point for the integrals belonging to the EFIE for (a) original and (b) proposed methods. A total of 128 quadrature sample points are considered for the test triangles, eight quadrature sample points in the angular direction, and 16 samples in the radial direction.

dependency on the shape of the test triangles, especially for the central $(x, y)$ positions. Moreover, the behavior is also reasonable even for the extremely deformed cases (close to the common vertices), demonstrating the method's applicability to arbitrarily shaped triangles in a realistic MoM example.

### C. Optimal Selection of the Quadrature Points

Having studied the stability of the proposed schemes for different relative positions between the test and source triangles and variations of the AR of the test triangle, a deeper analysis is next carried out to determine the feasibility of optimally selecting points to achieve a prescribed accuracy. Considering the stability demonstrated by the methods in the previous results, for the sake of conciseness, this study is carried out only for one of the examples presented for each triangle relationship: two triangles sharing a common vertex with a 15° vertex angle, two triangles sharing a common edge with a 90° vertex angle, and two triangles sharing their

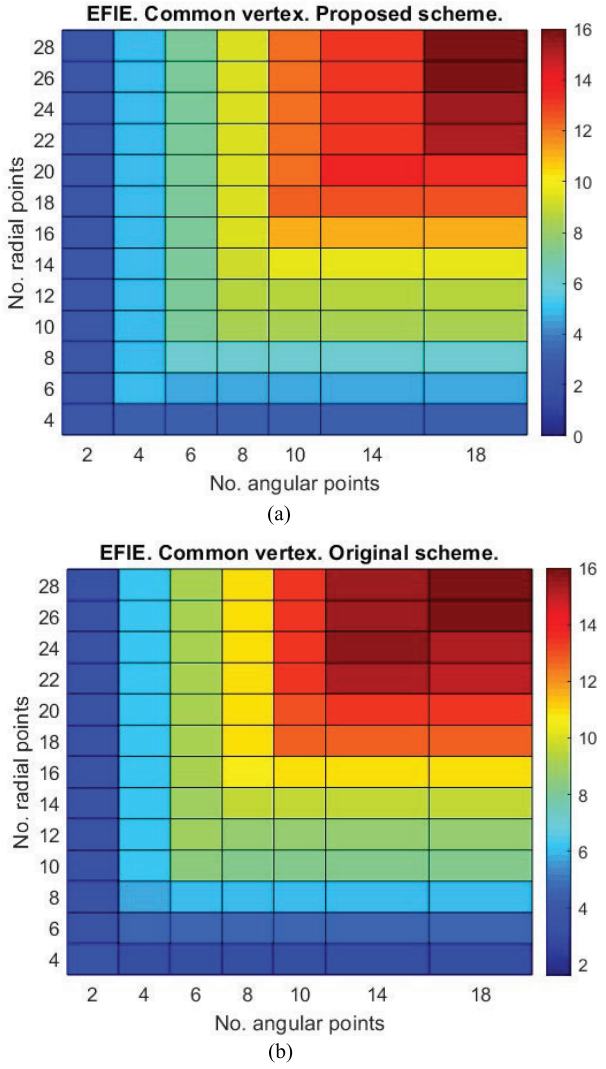


Fig. 20. Number of significant digits versus the number of quadrature points per linear dimension in angular and radial directions using (a) proposed and (b) original methods for the integrals belonging to the EFIE; coupling between triangles "1" and "5" in Fig. 11(b).

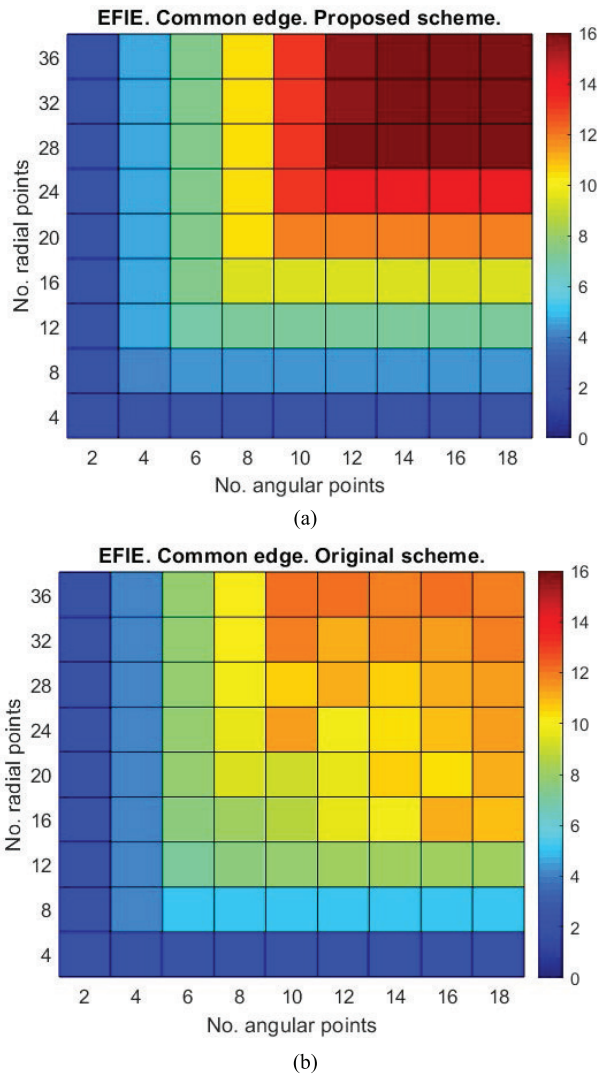


Fig. 21. Number of significant digits versus the number of quadrature points per linear dimension in angular and radial directions using (a) proposed and (b) original methods for the integrals belonging to the EFIE; coupling between triangles "1" and "3" in Fig. 11(a).

integration domains. We show in Fig. 20 how the accuracy of the EFIE integrals change relative to the number of radial and angular points for the proposed and original schemes applied to the common vertex case. Fig. 20 represents the number of significant digits as a matrix $[M]$ with respect to the number of radial and angular points. Each element of $[M]_{ij}$ shows the number of significant digits when applying the corresponding method with $i$ number of radial points and $j$ number of angular points. Hence, the rows and columns of $[M]_{ij}$ show the behavior of the accuracy when the sampling along one of the directions is fixed, suggesting, as expected, that the best performance is obtained by simultaneously increasing the sampling in both directions. We observe similar behavior between both methods, as shown in the first analysis for the common vertex case. It is also observed that the optimal relation between both linear dimensions is to approximately double the number of radial sample points compared to the angular ones.

Similar analyses are performed for the common edge case, with interesting results. For the proposed approach, in Fig. 21(a), we still see a linear relation between both directions, where the optimal case is obtained by setting the number of radial points to twice the number of angular points. In Fig. 21(b), this analysis is performed for the original scheme. It can be noticed that the performance is similar to the proposed scheme for low-to-moderate accuracies, but the convergence deteriorates for higher numbers of significant digits, as we lose the regular relationship between the number of angular and radial points and the optimum ratio becomes more difficult to predict. This behavior is also replicated in the self-term case since it is based on the common edge case, as can be observed in Fig. 22.

Finally, although these three configurations focused on isosceles triangles, the conclusions described above can be observed with other triangle shapes. For the sake of completeness, this analysis is extended for one of the very

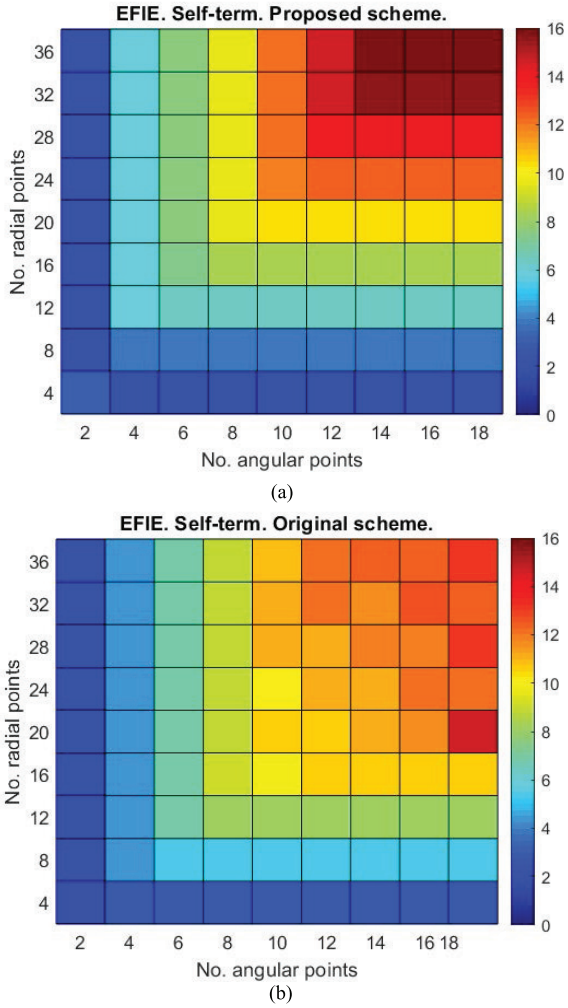


Fig. 22. Number of significant digits versus the number of quadrature points per linear dimension in angular and radial directions using (a) proposed and (b) original methods for the integrals belonging to the EFIE; self-coupling of triangle "1" in Fig. 11(a).

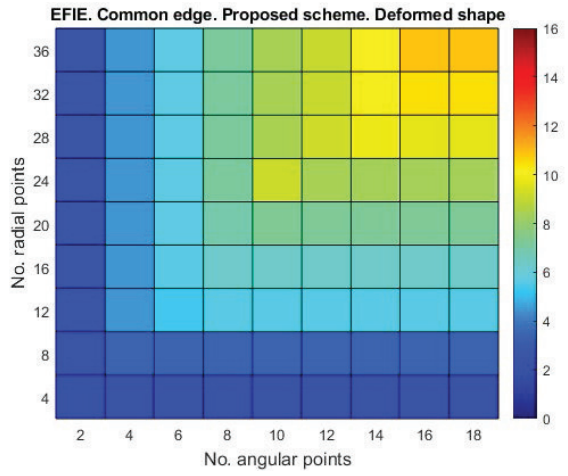


Fig. 23. Number of significant digits versus the number of quadrature points per linear dimension in angular and radial directions using the proposed method for the integrals belonging to the EFIE; coupling between triangles in Fig. 18 with the free vertex point located in position $(x, y) = (-0.4, 0.1)$.

deformed triangles shapes of triangles sharing a common edge shown in Fig. 18, with the free vertex located in position $(x, y) = (-0.4, 0.1)$. These results are shown in Fig. 23, where it can be verified that even if the reachable accuracy is lower, the number of radial points remains at about twice the number of angular points.

## VI. Conclusion and Perspectives

In this work, a novel test quadrature approach is proposed for the accurate evaluation of test (outer) integrals arising in moment methods, both for the EFIE and MFIE operators. The static behavior of the so-called vertex functions was studied and a custom quadrature scheme was developed that properly captures and accounts for the logarithmically singular behavior of potentials and their derivatives near edges and vertices using MRWlog quadrature and/or GL quadrature along the angular and radial dimensions, respectively. The new quadrature scheme has been formulated for the case of a test triangle sharing either a common vertex or a common edge with a source triangle, as well as for the self-term associated with the EFIE. Moreover, the proposed scheme is compared to and found to be similar in convergence properties to the original method of [12], which was applied only for the MFIE operator, but which, as shown here, applies to the evaluation of EFIE operators as well.

An analysis of the performance of the proposed method demonstrates its improved convergence, especially with respect to a conventional Gauss triangle scheme and, to a lesser extent, to the original method and the two methods described in [13]. The proposed approach yields essentially exponential numerical convergence to machine precision of 4-D MoM integrals. In this analysis, different triangle configuration pairs are considered, not only with respect to realistic angle scenarios between test and source triangles but also over a range of test triangle ARs that validate the generality of the proposed method. In addition, a preliminary study of the optimal selection of angular and radial points is included. Regarding the two methods proposed in [13], we remark that if only low accuracies are required in the EFIE integrals, their convergence is similar to the proposed approaches. However, those methods were not designed with the MFIE in mind, nor did they account for the strong angular variations of potentials near vertices. Finally, because of the near-exponential convergence (i.e., near-linear variation of the number of significant digits with respect to the number of sample points), the proposed method is generally more predictable in terms of selecting the number of sample points to achieve a prescribed accuracy.

The proposed method has been demonstrated to be a strong candidate for improving the accuracy and performance of the test integrals involved in the MoM for all the possible configurations and for both the EFIE and MFIE. Importantly, it may be easily integrated into any MoM code, independent of the source integration method (although, for high accuracy in the MoM matrix entries, the accuracy of both the inner and outer integrals must be considered together).

A possible next step is to extend the proposed integration scheme to higher order elements and basis functions and volumetric discretizations.

## ACKNOWLEDGMENT

The authors wish to thank Dr. Malcolm M. Bibby of Georgia Institute of Technology for providing extended tables for the MRWlog quadrature weights and sample points used in this study. They also appreciate the reviewers' thoughtful questions and insightful suggestions, all of which have contributed to improving the article's organization and clarity.

## REFERENCES

[1] D. Wilton, S. Rao, A. Glisson, D. Schaubert, O. Al-Bundak, and C. Butler, "Potential integrals for uniform and linear source distributions on polygonal and polyhedral domains," *IEEE Trans. Antennas Propag.*, vol. AP-32, no. 3, pp. 276–281, Mar. 1984.

[2] R. D. Graglia, D. R. Wilton, and A. F. Peterson, "Higher order interpolatory vector bases for computational electromagnetics," *IEEE Trans. Antennas Propag.*, vol. 45, no. 3, pp. 329–342, Mar. 1997.

[3] S. Rao, D. Wilton, and A. Glisson, "Electromagnetic scattering by surfaces of arbitrary shape," *IEEE Trans. Antennas Propag.*, vol. AP-30, no. 3, pp. 409–418, May 1982.

[4] M. A. Khayat and D. R. Wilton, "Numerical evaluation of singular and near-singular potential integrals," *IEEE Trans. Antennas Propag.*, vol. 53, no. 10, pp. 3180–3190, Oct. 2005.

[5] P. W. Fink, D. R. Wilton, and M. A. Khayat, "Simple and efficient numerical evaluation of near-hypersingular integrals," *IEEE Antennas Wireless Propag. Lett.*, vol. 7, pp. 469–472, 2008.

[6] M. A. Khayat, D. R. Wilton, and P. W. Fink, "An improved transformation and optimized sampling scheme for the numerical evaluation of singular and near-singular potentials," *IEEE Antennas Wireless Propag. Lett.*, vol. 7, pp. 377–380, 2008.

[7] F. Vipiana and D. R. Wilton, "Numerical evaluation via singularity cancellation schemes of near-singular integrals involving the gradient of helmholtz-type potentials," *IEEE Trans. Antennas Propag.*, vol. 61, no. 3, pp. 1255–1265, Mar. 2013.

[8] M. M. Botha, "Numerical integration scheme for the near-singular green function gradient on general triangles," *IEEE Trans. Antennas Propag.*, vol. 63, no. 10, pp. 4435–4445, Oct. 2015.

[9] L. Li and T. F. Eibert, "Radial-angular singularity cancellation transformations derived by variable separation," *IEEE Trans. Antennas Propag.*, vol. 64, no. 1, pp. 189–200, Jan. 2016.

[10] J. Rivero, F. Vipiana, D. R. Wilton, and W. A. Johnson, "Hybrid integration scheme for the evaluation of strongly singular and near-singular integrals in surface integral equations," *IEEE Trans. Antennas Propag.*, vol. 67, no. 10, pp. 6532–6540, Oct. 2019.

[11] A. G. Polimeridis, I. D. Koufogiannis, M. Mattes, and J. R. Mosig, "Considerations on double exponential-based cubatures for the computation of weakly singular Galerkin inner products," *IEEE Trans. Antennas Propag.*, vol. 60, no. 5, pp. 2579–2582, May 2012.

[12] F. Vipiana, D. R. Wilton, and W. A. Johnson, "Advanced numerical schemes for the accurate evaluation of 4-D reaction integrals in the method of moments," *IEEE Trans. Antennas Propag.*, vol. 61, no. 11, pp. 5559–5566, Nov. 2013.

[13] B. A. Freno, W. A. Johnson, B. F. Zinser, D. R. Wilton, F. Vipiana, and S. Campione, "Characterization and integration of the singular test integrals in the method-of-moments implementation of the electric-field integral equation," *Eng. Anal. Boundary Elements*, vol. 124, pp. 185–193, Mar. 2021.

[14] L. Gurel and O. Ergul, "Singularity of the magnetic field integral equation and its extractions," *IEEE Antennas Wireless Propag. Lett.*, vol. 4, pp. 229–232, 2005.

[15] O. Ergul and L. Gurel, "Improved testing of the magnetic-field integral equation," *IEEE Microw. Wireless Compon. Lett.*, vol. 15, no. 10, pp. 615–617, Oct. 2005.

[16] P. Yla-Oijala and M. Taskinen, "Calculation of cfie impedance matrix elements with RWG and n/spltimes/RWG functions," *IEEE Trans. Antennas Propag.*, vol. 51, no. 8, pp. 1837–1846, Aug. 2003.

[17] A. G. Polimeridis, F. Vipiana, J. R. Mosig, and D. R. Wilton, "DIRECTFN: Fully numerical algorithms for high precision computation of singular integrals in Galerkin SIE methods," *IEEE Trans. Antennas Propag.*, vol. 61, no. 6, pp. 3112–3122, Jun. 2013.

[18] E. H. Bleszynski, M. K. Bleszynski, and T. Jaroszewicz, "Reduction of volume integrals to nonsingular surface integrals for matrix elements of tensor and vector green functions of Maxwell equations," *IEEE Trans. Antennas Propag.*, vol. 61, no. 7, pp. 3642–3647, Jul. 2013.

[19] E. H. Bleszynski, M. K. Bleszynski, and T. Jaroszewicz, "Reduction of singular surface integrals to nonsingular line integrals in integral equations for planar geometries," *IEEE Trans. Antennas Propag.*, vol. 64, no. 11, pp. 4760–4769, Nov. 2016.

[20] D. R. Wilton, F. Vipiana, and W. A. Johnson, "Evaluation of 4-D reaction integrals in the method of moments: Coplanar element case," *IEEE Trans. Antennas Propag.*, vol. 65, no. 5, pp. 2479–2493, May 2017.

[21] D. Tihon and C. Craeye, "All-analytical evaluation of the singular integrals involved in the method of moments," *IEEE Trans. Antennas Propag.*, vol. 66, no. 4, pp. 1925–1936, Apr. 2018.

[22] J. Rivero, F. Vipiana, D. R. Wilton, and W. A. Johnson, "Evaluation of 4-D reaction integrals via double application of the divergence theorem," *IEEE Trans. Antennas Propag.*, vol. 67, no. 2, pp. 1131–1142, Feb. 2019.

[23] E. Bleszynski, M. Bleszynski, and T. Jaroszewicz, "The d'Alembertian representation of green's functions and evaluation of surface integrals over non-parallel planes," in *Proc. 18th Eur. Conf. Antennas Propag.*, 2024, pp. 4099–4102.

[24] K. A. Michalski and J. R. Mosig, "Multilayered media green's functions in integral equation formulations," *IEEE Trans. Antennas Propag.*, vol. 45, no. 3, pp. 508–519, Mar. 1997.

[25] I. Stevanovic, P. Crespo-Valero, K. Blagovic, F. Bongard, and J. R. Mosig, "Integral-equation analysis of 3-D metallic objects arranged in 2-D lattices using the Ewald transformation," *IEEE Trans. Microw. Theory Techn.*, vol. 54, no. 10, pp. 3688–3697, Oct. 2006.

[26] D. R. Wilton, J. Rivero, W. A. Johnson, and F. Vipiana, "Evaluation of static potential integrals on triangular domains," *IEEE Access*, vol. 8, pp. 99806–99819, 2020.

[27] J. Ma, V. Rokhlin, and S. Wandzura, "Generalized Gaussian quadrature rules for systems of arbitrary functions," Dept. Computer Science, Yale Univ., New Haven, CT, USA, Tech. Rep. YALEU/DCS/RR-990, Oct. 1993.

[28] J. Ma, V. Rokhlin, and S. Wandzura, "Generalized Gaussian quadrature rules for systems of arbitrary functions," *SIAM J. Numer. Anal.*, vol. 33, no. 3, pp. 971–996, Jun. 1996.

[29] J. Rivero, F. Vipiana, D. R. Wilton, and W. A. Johnson, "Novel test integral quadrature scheme for the method of moments," in *Proc. 17th Eur. Conf. Antennas Propag. (EuCAP)*, Mar. 2023, pp. 1–3.

[30] J. Rivero, V. F. Martín, D. R. Wilton, W. A. Johnson, and F. Vipiana, "Applying a novel testing scheme for the numerical evaluation of the magnetic field integral equation," in *Proc. IEEE Int. Symp. Antennas Propag.*, Portland, OR, USA, Jul. 2023, pp. 1211–1212.

[31] D. Tihon and C. Craeye, "Closed-form evaluation of the singular terms in electric field integral equations," in *Proc. 11th Eur. Conf. Antennas Propag. (EUCAP)*, Mar. 2017, pp. 520–524.

[32] J. A. Crow, "Quadrature of integrands with a logarithmic singularity," *Math. Comput.*, vol. 60, no. 201, p. 297, Jan. 1993.

[33] A. Van Oosterom and J. Strackee, "The solid angle of a plane triangle," *IEEE Trans. Biomed. Eng.*, vols. BME–30, no. 2, pp. 125–126, Feb. 1983.

[34] L. B. Zhang, T. Cui, and H. Liu, "A set of symmetric quadrature rules on triangles and tetrahedra," *J. Comput. Math.*, vol. 27, pp. 89–96, Jan. 2009.

**Javier Rivero** received the M.S. degree in telecommunication engineering from the Universidad Carlos III de Madrid, Getafe, Spain, in 2008, and the Ph.D. degree from the Universidad de Extremadura, Badajoz, Spain, in 2012.

He was a Research Assistant with the Universidad de Extremadura, Badajoz, from 2012 to 2017 and Politecnico di Turin, Turin, Italy, from 2018 to 2022, where he also conducted a Post-Doctoral Researcher from 2015 to 2017. From 2017 to 2018, he was with the Istituto Superiore Mario Boella (ISMB), Turin. Since 2022, he has been a Senior Engineer with Sandia National Laboratories, Albuquerque, NM, USA. His research interests include fast integral equation methods, method-of-moments approaches, metamaterials, nanoplasmonics, Green's function regularization, advanced integration schemes, periodic Green's functions, and high-$Q$ cavities.

**Víctor F. Martín** (Member, IEEE) received the M.S. degree in telecommunication engineering and the Ph.D. degree from the University of Extremadura, Badajoz, Spain, in 2019 and 2022, respectively.

In 2023, he was a Post-Doctoral Researcher with the Department of Electronics, Politecnico di Torino, Turin, Italy, and the Department of Signal Theory and Communications, University of Vigo, Vigo, Spain, in 2024. Since September 2024, he has been an Assistant Professor with the Department of Signal Theory and Communications and Telematic Systems and Computing, Universidad Rey Juan Carlos, Madrid, Spain. His research interests include fast integral equation methods, domain decomposition techniques and supercomputing techniques in computational electromagnetics, electromagnetic compatibility, and analysis of nano-optical devices.

**Donald R. Wilton** (Life Fellow, IEEE) received the B.S., M.S., and Ph.D. (under a Hughes Doctoral Fellowship) degrees in electrical engineering from the University of Illinois Urbana–Champaign, Champaign, IL, USA, in 1964, 1966, and 1970, respectively.

From 1965 to 1968, he was with Hughes Aircraft Company, Fullerton, CA, USA. From 1970 to 1983, he was with the Department of Electrical Engineering, University of Mississippi, Oxford, MS, USA. From 1983 to 2012, he was with the University of Houston, Houston, TX, USA, retiring as a Professor Emeritus with the Department of Electrical and Computer Engineering. His primary research area is computational electromagnetics. He has published, lectured, and consulted extensively in this area.

Dr. Wilton is a member of the National Academy of Engineering, the IEEE Antennas and Propagation Society, and Commissions B and E of the International Radio Science Union (URSI). He was a recipient of the IEEE Third Millennium Medal in 2000 and the IEEE Electromagnetics Award in 2015. He was an inaugural recipient of the Applied Computational Electromagnetics Society (ACES) Computational Electromagnetics Award in 2013 and the IEEE AP-S Harrington-Mittra Award in Computational Electromagnetics in 2014. He has served both organizations in various capacities, including as an IEEE AP-S Distinguished National Lecturer from 1984 to 1986.

**William A. Johnson** (Senior Member, IEEE) received the B.S., M.A., and Ph.D. degrees in mathematics with minor in physics from the University of Arizona, Tucson, AZ, USA, in 1972, 1974, and 1978, respectively.

His work experience includes Sandia National Laboratories, Albuquerque, NM, USA, where he was a Distinguished Member of the Technical Staff, Lawrence Livermore National Laboratory, University of Mississippi, Oxford, MS, USA, and an Adjunct Associate Professor of mathematics with the University of New Mexico, Albuquerque, NM, USA. He was a Visiting Assistant Professor of mathematics with New Mexico Institute of Mining and Technology, Socorro, NM, USA, from 2016 to 2107.

Dr. Johnson is a Full Member of URSI Commission B.

**Francesca Vipiana** (Senior Member, IEEE) is a Full Professor of electromagnetic fields with the Department of Electronics and Telecommunications, Politecnico di Torino, Turin, Italy. Her research activities concern numerical techniques based on integral equations and method of moments, and the modeling, design, realization, and testing of microwave imaging and sensing systems for medical and industrial applications.

Dr. Vipiana is a member of the EurAAP Board of Directors. She received the Lot Shafai Mid-Career Distinguished Award from the IEEE Antennas and Propagation Society (AP-S) in 2017. She was an Associate Editor of IEEE TRANSACTIONS ON ANTENNAS AND PROPAGATION from 2018 to 2024 and the Founder and responsible for the Women in Engineering Column in *IEEE Antennas and Propagation Magazine* from 2019 to 2024. She is the Vice-Chair of the IEEE AP-S Diversity, Equity, Inclusion and Sense of Belonging Committee.